



# Improved durability and activity of Pt/C catalysts through atomic layer deposition of tungsten nitride and subsequent thermal treatment

W. Wilson McNeary<sup>a</sup>, Sarah F. Zaccarine<sup>b</sup>, Annika Lai<sup>a</sup>, Audrey E. Linico<sup>a</sup>, Svitlana Pylypenko<sup>b</sup>, Alan W. Weimer<sup>a,\*</sup>

<sup>a</sup> Department of Chemical and Biological Engineering, University of Colorado Boulder, Boulder, CO, 80303, USA

<sup>b</sup> Department of Chemistry, Colorado School of Mines, Golden, CO, 80401, USA

## ARTICLE INFO

### Keywords:

Atomic layer deposition  
Fuel cells  
Oxygen reduction reaction  
Tungsten nitride  
Catalysis  
Nanomaterials

## ABSTRACT

Atomic layer deposition (ALD) of tungsten nitride (WN) enhanced the durability and activity of a carbon-supported Pt nanoparticle oxygen reduction reaction (ORR) catalyst by adding protective WN nanostructures to the surface. A post-synthesis thermal treatment sequence of low-temperature oxidation followed by high-temperature reduction was carried out on the ALD-modified catalyst. The effects of the ALD process and thermal treatment on the structure and electrochemical properties of the catalyst were examined. Characterization through ICP-MS, STEM and EDS mapping, and X-ray diffraction showed that the ALD process deposited WN homogeneously across the surface. Thermal treatment resulted in a reduced amount of nitride on the surface and produced separate Pt and W domains. The electrochemical performance of the catalysts is measured through rotating disk electrode voltammetry. The thermally-treated ALD catalyst was observed to have a high mass activity towards the ORR (465 mA/mg), surpassing benchmark Pt/C (277 mA/mg), and demonstrated superior retention of electrochemical properties after an accelerated durability test. Analysis of particle size distributions before and after durability testing also indicated that the mechanical stability of the Pt nanoparticles is enhanced in the thermally-treated ALD catalyst compared to the uncoated materials.

## 1. Introduction

The development of sufficiently active, durable, and cost-effective catalysts for the cathodic oxygen reduction reaction (ORR) is a major bottleneck in the commercialization of polymer electrolyte membrane fuel cells (PEMFCs) [1]. Conventional carbon-supported Pt nanoparticle catalysts (Pt/C) can provide high surface areas and moderate activities; however, these materials are prone to performance degradation during fuel cell operation through Pt crystallite migration, electrochemical Ostwald ripening, and carbon support corrosion [2,3]. As these degradation pathways are promoted by voltage perturbations induced during vehicle operation and the acidic environment of the PEMFC, it is essential to develop durable catalysts that can withstand these harsh operating conditions.

One promising approach to increasing the durability of Pt/C ORR catalysts is the stabilization of Pt nanoparticles through the addition of blocking structures, which are typically comprised of acid-stable metal oxides that mitigate Pt migration and agglomeration. These may be integrated during wet chemistry synthesis of catalyst [4–7] or added to the particulate support material by atomic layer deposition (ALD) in a

post-synthesis step [8]. ALD is a self-limiting vapor-phase process that offers atom-level control over the growth of metal oxide films or metal nanoparticles by varying the number of surface reaction steps, or “cycles” [9]. Protective layers deposited onto metal nanoparticle catalysts for high-temperature reactions via ALD have been shown to preserve activity and prevent thermally-induced sintering and loss of active surface area [10–13]. ALD has also been shown to be a versatile technique for the synthesis and modification of ORR catalysts for PEMFCs [14]. Recently, the addition of ALD metal oxide nanostructures, such as ZrO<sub>2</sub> [15], SnO<sub>2</sub> [16], TiO<sub>2</sub> [17,18], and nitrogen-doped Ta<sub>2</sub>O<sub>5</sub> [19] onto Pt/C ORR catalysts has shown great promise for improving retention of electrochemical surface area (ECSA), activity, and Pt nanoparticle size retention over electrochemical durability testing. In addition to increased durability, the proximity of these ALD blocking structures to the Pt may also enhance activity through beneficial metal support interactions [6,15] or alloying effects after subsequent thermal treatment [17,20]. Tungsten nitride (WN) has been previously investigated as both an ORR co-catalyst and support material with promising results [21,22], but has not been investigated as an ALD blocking agent for Pt/C. The corrosion resistance of WN under acidic

\* Corresponding author.

E-mail address: [alan.weimer@colorado.edu](mailto:alan.weimer@colorado.edu) (A.W. Weimer).

<https://doi.org/10.1016/j.apcatb.2019.05.036>

Received 2 November 2018; Received in revised form 8 March 2019; Accepted 8 May 2019

Available online 09 May 2019

0926-3373/ © 2019 Elsevier B.V. All rights reserved.

and oxidizing conditions, along with its potential synergistic effects on Pt catalyst activity, make it an attractive candidate for stabilization of Pt-based ORR catalysts.

In this work, we report modification of a catalyst synthesized in-house through Pt-H<sub>2</sub> ALD on a functionalized carbon black substrate (ALD Pt/f-C) [23] with WN nanostructures. To our knowledge, this is the first report of this particular ALD chemistry being applied to any type of Pt/C ORR catalyst. The ALD Pt/f-C catalyst was selected for this study because of the high amount of O-containing groups available on the functionalized carbon, which facilitate enhanced ALD growth rates over an unmodified carbon substrate. Ten cycles of WN ALD were applied to the Pt/f-C catalyst. This material was subsequently treated with a 200 °C oxidation to remove residual Pt-H<sub>2</sub> ALD ligands [17], followed by a 725 °C anneal in 20% H<sub>2</sub> to reduce deposited WN to metallic W. As-prepared catalysts were examined through elemental analysis, X-ray diffraction, and electron microscopy and the effects of WN ALD and thermal treatment on electrochemical activity and durability were characterized using rotating disk electrode (RDE) techniques.

## 2. Experimental

### 2.1. Catalyst synthesis

WN ALD structures were added to the ALD Pt/f-C catalyst using bis(*tert*-butylimido)bis(dimethylamido)tungsten ((<sup>t</sup>BuN)<sub>2</sub>(Me<sub>2</sub>N)<sub>2</sub>W; Strem) and ammonia (Sigma-Aldrich) as alternating reagents in a fluidized bed reactor. In a single ALD cycle, the ((<sup>t</sup>BuN)<sub>2</sub>(Me<sub>2</sub>N)<sub>2</sub>W dose was held for 13 min, and the NH<sub>3</sub> was held for 20 min. Gases were purged between half-cycles with UHP N<sub>2</sub>. The reactor and reactant bubbler were held at 300 °C and 40 °C, respectively. This WN ALD process was adapted from previous studies on flat substrates, [24,25] as it has never been attempted in a fluidized bed setup. An in-line mass spectrometer (Stanford Research Systems) was used to monitor gases exiting the reactor. Ten ALD cycles were deposited to produce catalyst 10 WN. The 10 WN catalyst was subjected to a 200 °C oxidation in air for 3 h, followed by a 725 °C anneal in 20% H<sub>2</sub> with balance Ar for 3 h to produce material 725 °C-10WN for further analysis.

### 2.2. Analytical characterization

ALD Pt/f-C and 10 WN were analyzed for Pt and W content using inductively coupled plasma mass spectroscopy (ICP-MS) after digestion in an aqua regia/HF mixture. Bright field microscopy images of catalysts before and after electrochemical durability testing were acquired by depositing catalyst powder on carbon film 200 mesh copper grids (Electron Microscopy Sciences) and examining under a TEM (FEI Tecnai T12 Spirit). Particle size distributions were tabulated from these images using ImageJ, in which Feret diameters were calculated from a total of 200 Pt nanoparticles taken from 3 separate areas of the catalyst. Feret diameters initially and after durability testing were compared using a *t*-test assuming unequal variance. Dark field and bright field microscopy and energy dispersive X-ray spectroscopy (EDS) mapping are performed on as-synthesized catalysts by depositing catalyst powder on carbon film 200 mesh copper grids (Ted Pella) using a transmission electron microscope (TEM) operated at 200 kV in scanning mode (FEI Talos F200X). Powder x-ray diffraction (XRD) measurements were collected using a Bruker D2 Phaser with a Cu source operating at 300 W and a Lynxeye 1D detector.

### 2.3. Electrochemical characterization

Ink dispersions were made from the catalyst powders using ultrapure water, isopropyl alcohol (Sigma-Aldrich), and 5% Nafion ionomer (Sigma-Aldrich). After a 1 h sonication, a 10 µL aliquot of ink was drop-coated onto a glassy carbon electrode and rotated at 700 rpm in an inverted position on a RDE test stand (Pine). After drying, the working

electrode was submerged in an aqueous electrochemical cell (0.1 M HClO<sub>4</sub>) with a Pt coil counter electrode and regular hydrogen electrode (RHE) reference. Data acquisition procedures followed those established by Shinzaki, et al [26]. After a 100 cycle break-in (0.025–1.2 V at 500 mV s<sup>-1</sup>), cyclic voltammograms (CVs) were taken from 0.025 to 1.0 V at 10 mV s<sup>-1</sup> in an N<sub>2</sub>-purged cell with no rotation. The calculated hydrogen under potential deposition (*H<sub>UPD</sub>*) charge from 0.06 to 0.4 V was used to calculate the electrochemical surface area (ECSA). Polarization curves were taken from 1.0 to -0.01 V at 20 mV s<sup>-1</sup> in an O<sub>2</sub>-purged cell at 1600 rpm and the anodic scan is used for analysis. Background curves were taken with the same parameters under N<sub>2</sub> and used to correct the polarization curves. Kinetic current (*I<sub>k</sub>*) was determined according to Eq. (1), using the current at 0.9 V (*I*) and the mass-transfer limited current (*I<sub>lim</sub>*), taken at 0.4 V. Mass activities (*i<sub>m0.9V</sub>*) were then calculated by normalizing *I<sub>k</sub>* by the mass loading of Pt on the electrode. ECSA and mass activity were calculated initially and after an accelerated durability test (ADT) of 5000 voltage cycles from 0.6 to 1.2 V at 100 mV s<sup>-1</sup> adapted from [16].

$$I_k = \frac{I_{lim} \times I}{I_{lim} - I} \quad (1)$$

## 3. Results and discussion

A representative mass spectrometry trace during a single WN ALD cycle is shown in Fig. 1. The emergence of signals corresponding to the ((<sup>t</sup>BuN)<sub>2</sub>(Me<sub>2</sub>N)<sub>2</sub>W fragments shown at ~25 min was indicative of saturation of the available surface sites; therefore, the metal precursor dose was ended upon the appearance of these fragments. The NH<sub>3</sub> dose shown at ~65 min was marked by a rapid rise in the same fragments due to ligand composition (as detailed in [25]), and the dose was held for 20 min. Elemental analysis with ICP-MS of the original and post-ALD catalysts (Table 1) showed the addition of 6.33 wt% W after 10 ALD cycles.

STEM images and corresponding EDS maps for 10 WN and 725 °C-10 WN are shown in Fig. 2. EDS quantification values are listed in Table 2. Additional images and EDS maps for 10 WN, 200 °C-10 (the intermediate stage of thermal treatment), and 725 °C-10 WN are provided in Fig. S11-4. Analysis of the 10 WN EDS maps showed the homogeneous presence of Pt, W, and N across the surface. The ALD Pt/f-C surface was initially covered in dispersed 2–3 nm Pt nanoparticles; the significant overlap between W and Pt in 10 WN showed that, during the ALD process, WN was deposited evenly throughout the Pt nanoparticles. The further overlap between N and W confirmed the presence of a nitride species. The functionalized carbon substrate of ALD Pt/f-C has previously been demonstrated to facilitate TiO<sub>2</sub> ALD surface reactions [17], as it provides O-terminated sites for nucleation and growth.

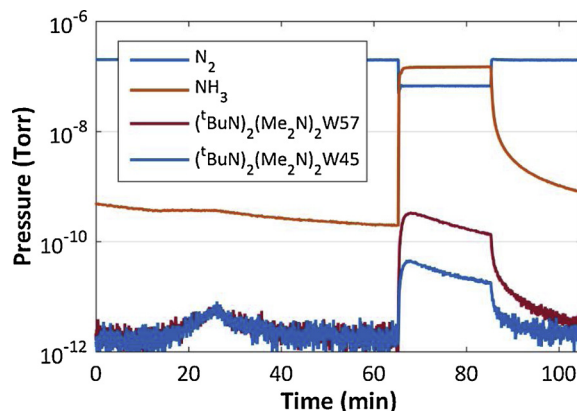
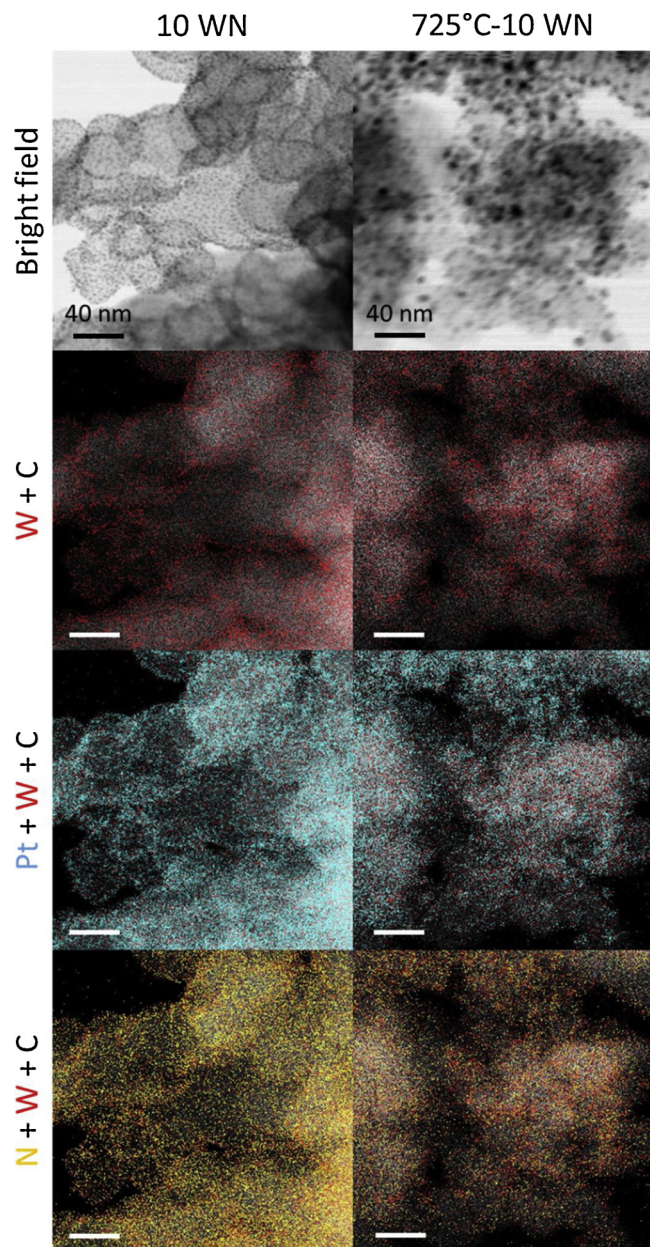


Fig. 1. Time-resolved mass spectrometry traces of *m/z* = 28 (N<sub>2</sub>), 17 (NH<sub>3</sub>), 45, and 57 ((<sup>t</sup>BuN)<sub>2</sub>(Me<sub>2</sub>N)<sub>2</sub>W fragments) during one WN ALD cycle.

**Table 1**  
Elemental content of ALD Pt/f-C and 10 WN catalysts as determined by ICP-MS.

	Pt wt%	W wt%
ALD Pt/f-C	19.8	–
10 WN	16.0	6.33



**Fig. 2.** Bright field STEM images and corresponding EDS overlays of elemental maps showing the distribution of Pt, C, W, and N in 10 WN and 725 °C-10 WN samples.

**Table 2**  
EDS quantification of W, Pt, N, and C on an atomic basis.

	W at%	Pt at%	N at%	C at%
10 WN	0.25	1.83	0.84	95.01
725 °C-10 WN	0.73	1.68	0.39	95.83

The f-C carbon substrate was similarly active towards the WN ALD process performed here.

Thermal treatment at 725 °C under 20% H<sub>2</sub>/Ar induced a number of structural changes in the catalyst. Coarsening of the Pt nanoparticles following thermal treatment was apparent in the bright field images of 725 °C-10 WN and corresponding Pt maps. Interestingly, it appeared that W was also slightly agglomerated during thermal treatment, but not to the same extent as Pt. The W map of 725 °C-10 WN still showed dispersed W across the surface, though its presence was reduced at the edges of the carbon particles. The combined overlay of Pt and W showed distinct W-rich areas (shown in red) present between the Pt clusters (shown in blue) and less correlation between the positions of Pt and W after thermal treatment than before. These results indicate that the Pt and W species remained in mostly separate phases in the 725 °C-10 WN catalyst and the thermal treatment likely did not produce alloy or intermetallic nanoparticles, as has often been observed with other Pt-W nanoparticle catalysts synthesized by colloidal or galvanic replacement methods [27,28]. A significant decrease in the presence of N across the surface can be observed from 10 WN to 725 °C-10 WN in the N + W maps in Fig. 2; this is also reflected by the decrease in N at% in Table 2 between the two catalysts. The W:N atomic ratio of 10 WN increased from 0.3 to almost 1.9 after thermal treatment, which indicates that the partial hydrogen atmosphere of the thermal treatment significantly changed the stoichiometry of the WN nanostructures. This process created a catalyst surface in 725 °C-10 WN with more metallic character but did not completely eliminate the presence of N.

All catalysts were probed with X-ray diffraction, and the results are shown in Fig. 3, alongside normalized XRD patterns for Pt, W, and WN [29,30]. The XRD pattern for ALD Pt/f-C catalyst showed broad Pt peaks around 39° and 46°, with a broad amorphous carbon peak near 25°. The addition of 10 WN ALD cycles did not result in any discernable changes in the 10 WN pattern. Though the presence of WN in this catalyst was previously confirmed through ICP-MS and STEM-EDS, it is possible that the quantity of WN on the surface was not large enough to produce a distinct reflection during the XRD analysis. Additionally, thermal ALD processes, such as the one followed here, are known to deposit amorphous materials; thus, the WN present in the 10 WN catalyst was likely not crystalline and would not be expected to produce large XRD peaks. Application of thermal treatment greatly increased the sharpness and intensity of the Pt peaks in the 725 °C-10 WN pattern. This was attributed to the Pt coarsening observed in the bright field images in Fig. 2. Also noteworthy is the relatively unchanged position of the Pt peak at 39° after thermal treatment. This indicates that the Pt lattice was not detectably compressed by the surrounding W on the

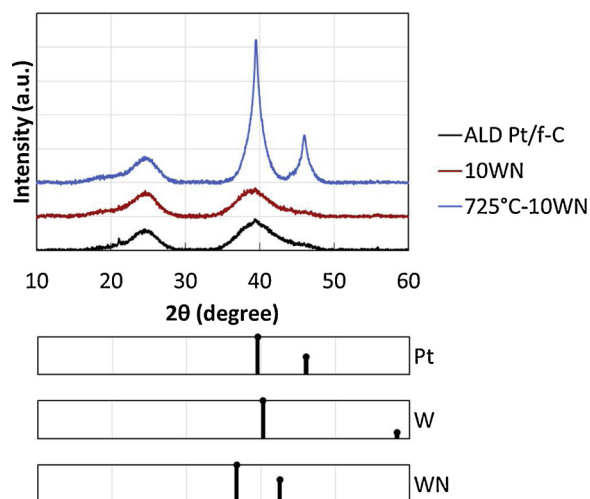


**Fig. 3.** XRD patterns of all catalysts. Normalized XRD patterns for Pt, W, and WN are shown below the data.

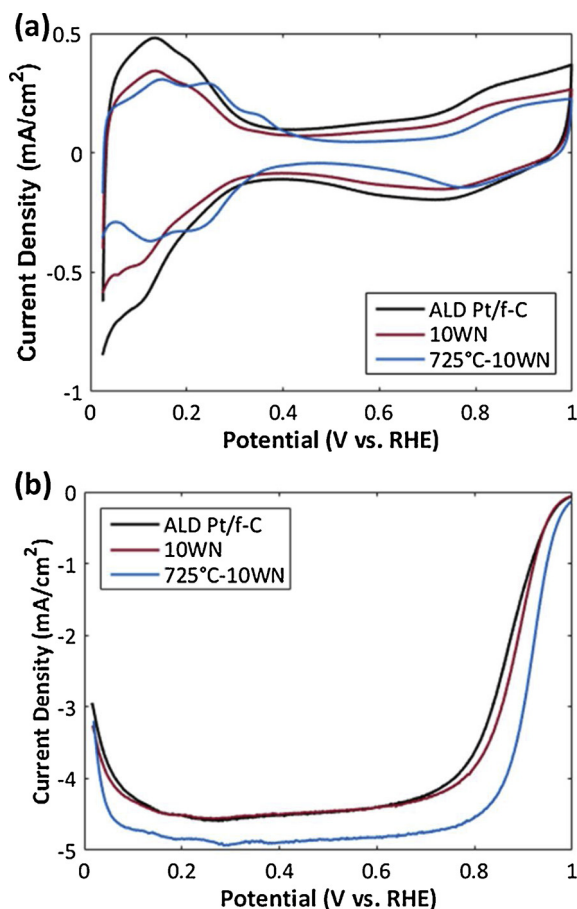


Fig. 4. Initial cyclic voltammograms (a) and polarization curves (b) for all ALD catalysts.

surface, which supports the assertion that Pt and W remain primarily in separate phases. The 725 °C-10 WN pattern does not show any distinct reflections for W, despite an increased presence of metallic W (as seen in Fig. 2) and a high likelihood that any W/WN species would exist in a crystalline phase by 725 °C. This may be due to insufficient quantities of W for detection through this technique, or the presence of the primary W peak at 40° may be obscured by the larger Pt reflection at 39°.

Electrochemical performance of the catalysts was assessed through RDE voltammetry. Initial cyclic voltammograms (CVs) and polarization curves for ALD Pt/f-C, 10 WN, and 725 °C-10 WN are shown in Fig. 4. An apparent decrease in the magnitude of the Pt  $H_{UPD}$  peak was observed for 10 WN and 725 °C-10 WN as shown in Fig. 4(a). This decrease was likely due to Pt nanoparticle coarsening during ALD and thermal treatment; however, ECSA values for these catalysts were actually greater than ALD Pt/f-C after accounting for changes in Pt content with the addition of ALD (see Fig. 5(a)). The CV for 725 °C-10 WN exhibited a sharply-defined peak in the more positive potential region of the  $H_{UPD}$  (0.2 – 0.3 V) that was not prominent in the other catalysts. This peak is associated with strongly adsorbed hydrogen species on the Pt(100) surface [31,32], and its emergence in the CV indicates that thermal treatment and the resultant Pt nanoparticle coarsening exposed more of this particular facet than was present in the initial catalysts. The CV for 725 °C-10 WN also showed a positive shift in the oxygen adsorption/desorption peaks relative to the other catalysts, indicating that oxygenated species do not bind as tightly to the 725 °C-10 WN catalyst sites. Finally, the 725 °C-10 WN catalyst also exhibited the lowest double layer capacitance contribution in its CV, likely due to the elimination of any residual O-containing surface groups on the functionalized carbon substrate during thermal treatment.

The initial polarization curves in Fig. 4(b) showed relatively similar

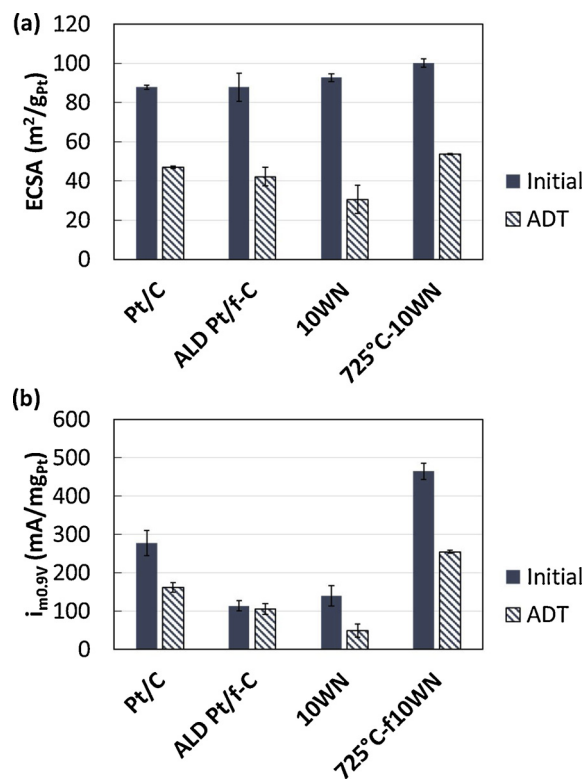
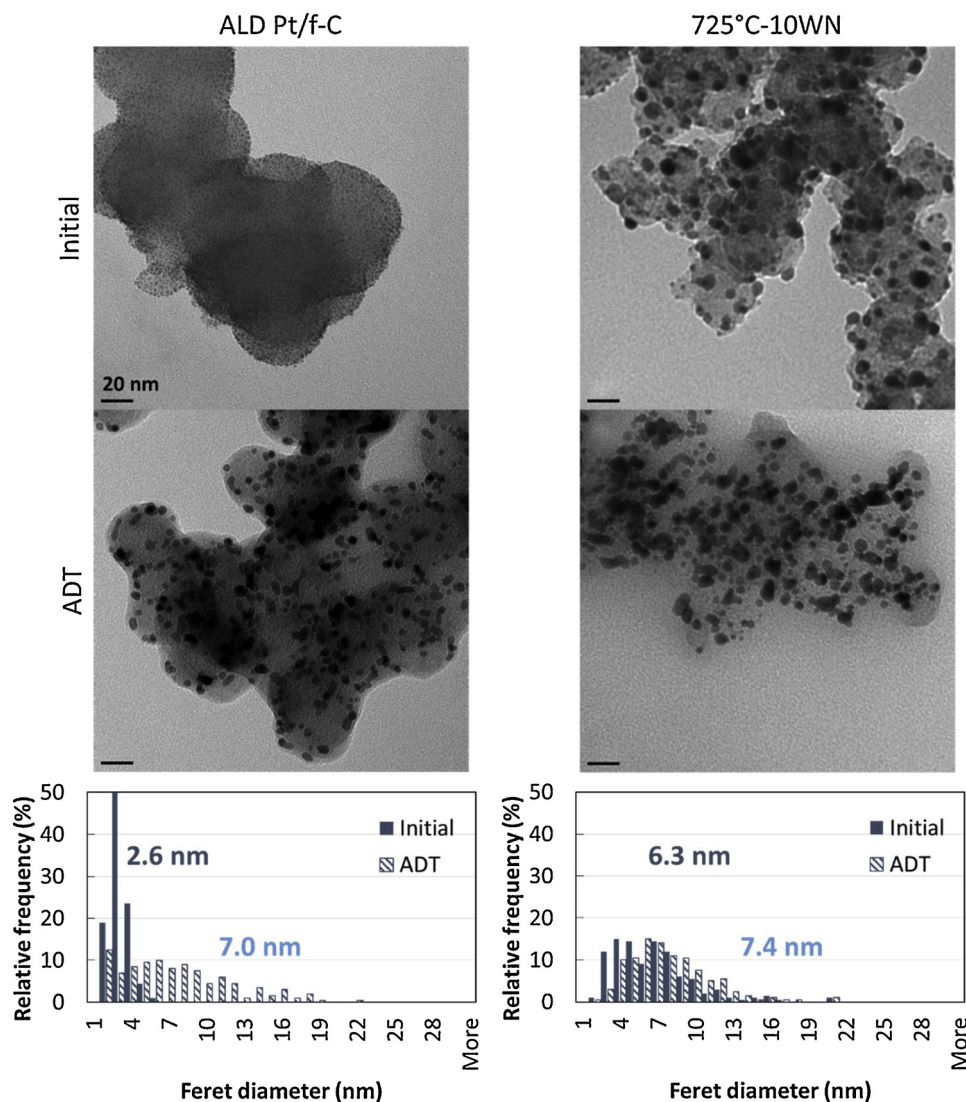


Fig. 5. Electrochemical surface areas (a) and mass activities (b) of all catalysts initially and after a 5000 voltage cycle durability test (ADT).

ORR performance for ALD Pt/f-C and 10 WN, though 10 WN was slightly more active due to a more positive half-wave potential. Thermal treatment resulted in a significantly more positive half-wave potential as well as an increased limiting current for the 725 °C-10 WN catalyst. A portion of this catalytic enhancement (primarily, the increase in limiting current) can be attributed to the removal of residual Pt-H<sub>2</sub> ALD ligands during the first phase of thermal treatment (200 °C oxidation in air), as is shown in Fig. S15. This behavior has previously been observed for the ALD Pt/f-C catalyst [17]. However, the majority of the increase in half-wave potential occurred after treatment of the catalyst at 725 °C under 20% H<sub>2</sub>. An additional control experiment in which the ALD Pt/f-C was exposed to similar conditions of 700 °C under 20% H<sub>2</sub> (Fig. S17; Table S11) showed that thermal treatment alone was not responsible for the full half-wave potential increase; the presence of ALD-deposited tungsten species in 725 °C-10 WN was essential for its superior ORR performance. This indicates that the catalytic activity was distinctly enhanced by the creation of W-rich nanostructures in close proximity to the larger Pt nanoparticles of 725 °C-10 WN, as observed in Fig. 2. One potential cause for this enhancement may be the modification of adsorption strength of oxygen-based ORR intermediates via synergistic interactions between the W/WN species and Pt. The previously-discussed CV results support the assertion that binding strength of oxygenated species is weakened in 725 °C-10 WN. Even though XRD results do not indicate significant Pt lattice strain in 725 °C-10 WN, it is possible that a d-band shift was induced in Pt through strong electronic ligand effects, which have been previously observed in Pt-W ORR catalysts [27]. There are numerous other reports in the literature detailing the catalytic influence of W-containing species in close proximity to Pt for ORR [22,33,34], as well for other reactions, such as toluene hydrogenation [35]. It is also possible that excess nitrogen atoms (either present on the N-rich surface after ALD or liberated from the WN) may have been doped into the carbon support during the 725 °C treatment, thereby leading to improved catalytic activity [36] regardless of the relationship between the W and Pt species. Though the current results



**Fig. 6.** TEM images for ALD Pt/f-C and 725 °C-10 WN catalysts initially and after durability testing (ADT). Particle size distributions tabulated from multiple images are shown below along with mean initial and ADT nanoparticle diameters.

clearly document a substantial increase in ORR performance with application of a thermal treatment, further characterization is required to discern the precise nature of the observed catalytic enhancement in 725 °C-10 WN and its causal factors.

The electrochemical durability of the catalysts was assessed using an accelerated durability test; results of this analysis for ECSA and mass activity are presented in Fig. 5. The performance of the ALD catalysts was benchmarked against a commercial Pt/C (Premetek P10A200). All catalysts were observed to lose ECSA over voltage cycling, with 725 °C-10 WN proving the most robust. Similarly, 725 °C-10 WN had the best performance in mass activity over the durability test, starting with the highest value reported in the current study for any catalyst, 465 mA/mg, and retaining 55% of that over voltage cycling. The initial mass activity of 725 °C-10 WN was considerably higher than that of commercial Pt/C, and its ADT value was on par with the initial activity of Pt/C. The enhanced durability of this catalyst is likely due to the stabilization of the Pt nanoparticles by nearby W/WN species on the carbon substrate. At first glance, the ALD Pt/f-C appeared to have superior retention of mass activity as a percentage of its initial value; however, this does not comport with the catalyst's observed ECSA loss. The apparent mass activity retention of ALD Pt/f-C was previously established to be an artifact of the residual Pt-H<sub>2</sub> ALD ligands on its surface [17] and is the result of simultaneous oxidation of the ligands

(activity increase) and Pt nanoparticle sintering (ECSA/activity decrease) during voltage cycling. Surprisingly, the 10 WN catalyst appeared to have the worst durability in regards to ECSA and mass activity, despite the addition of 10 cycles of WN ALD. This indicates that the as-deposited WN was not stable in the acidic environment under voltage cycling (perhaps due to its as-deposited amorphous state), and thermal treatment is necessary to realize any durability benefits from the deposited materials.

In order to further analyze the effects of voltage cycling on Pt nanoparticle stability, TEM images of the ALD Pt/f-C and 725 °C-10 WN catalysts were analyzed to generate particle size distributions initially and after durability testing. Representative TEM images initially and after durability testing are shown in Fig. 6, along with particle size distributions for each catalyst. Additional TEM images are provided in Figs. SI8 and SI9. Results of statistical analyses on the initial and ADT particle size distributions are provided in Tables SI2 and SI3. A significant shift, from a narrow initial distribution with a mean diameter of 2.6 nm to a much wider distribution with a mean diameter of 7.0 nm after the durability test, was shown for ALD Pt/f-C in Fig. 6. This is reflective of the catalyst's large ECSA loss and is the expected behavior for unprotected Pt nanoparticles over voltage cycling. The initial distribution for 725 °C-10 WN shown in Fig. 6 has a mean diameter of 6.3 nm, which shows that thermal treatment resulted in the

considerable growth of the Pt nanoparticles from their original size. However, the durability test only resulted in a slight shift in the distribution, producing an ADT mean diameter of 7.4 nm. This change in the particle size was also statistically significant, but considerably smaller in magnitude than that observed for the unmodified catalyst. Some of this improvement in particle size retention may be attributable to the larger initial mean diameter for 725 °C-10 WN, as larger particles do not have as strong of a driving force to minimize surface energy and will be less prone to coalescence. However, analysis of the particle size distributions for commercial Pt/C (Fig. SI10), which had an initial mean diameter of 5.3 nm—much closer to that of 725 °C-10 WN—shows that the Pt nanoparticles in 725 °C-10 WN were more stable and retained a smaller ADT mean diameter than Pt/C. In the control case of thermally-treated ALD Pt/f-C (Fig. SI11), which also had a comparatively large initial mean diameter of 4.8 nm, the unprotected nanoparticles agglomerated to a greater extent than those of 725 °C-10 WN did over potential cycling. Taken together, these results provide further evidence of the enhanced stability of the Pt nanoparticles in the 725 °C-10 WN catalyst. The most likely source of this enhanced stability was the steric confinement provided by the stable W/WN nanostructures that were shown to reside in close proximity to the Pt nanoparticles on this catalyst. The presence of these structures likely inhibited migration and coalescence of the Pt nanoparticles across the carbon surface over potential cycling, though the structures did not appear to completely eliminate nanoparticle coarsening. It is possible that other catalyst degradation routes under voltage cycling, such as electrochemical Ostwald ripening and carbon corrosion, remained active in the ALD-modified catalysts due to the relatively small amount of W added after 10 ALD cycles. Taken alongside the electrochemical durability data reported above, these results show that WN ALD and subsequent thermal treatment greatly enhance the ORR activity and durability of a previously unremarkable Pt/f-C catalyst.

#### 4. Conclusions

Atomic layer deposition of WN and subsequent thermal treatment were used to enhance the activity and durability of an ALD Pt/f-C catalyst. It was observed that WN grew readily on the functionalized carbon substrate during the ALD process, depositing 6.33 wt% W after 10 ALD cycles. The WN nanostructures were homogeneously dispersed across the catalyst surface after ALD. Thermal treatment consisting of a 200 °C oxidation in air followed by a 725 °C treatment under 20% H<sub>2</sub> was seen to result in coarsening of the Pt nanoparticles, while the W on the surface remains dispersed and did not appear to form an alloyed phase with Pt. However, thermal treatment did change the character of the WN nanostructures by reducing the amount of N present, which resulted in a more W-rich surface. The thermally-treated catalyst was found to have vastly superior activity towards the ORR than both the unmodified catalyst and the catalyst after 10 cycles of WN ALD; it also outperformed a benchmark Pt/C catalyst. This was attributed to synergistic metal-support effects induced by the W/WN nanostructures' proximity to the Pt nanoparticles. The thermally-treated catalyst also exhibited superior electrochemical durability and retention of Pt nanoparticle size over accelerated durability testing due to the stabilizing effects of the W/WN structures. By examining the beneficial electrocatalytic effects of an ALD chemistry previously untested for this application, this work further demonstrates the utility of ALD in the modification of Pt/C ORR catalysts.

#### Conflict of interest

A.W. Weimer has a significant financial interest in ALDNanosolutions, Inc.

#### Acknowledgments

The authors would like to thank Fredrick Luiszer for ICP-OES analysis. WWM gratefully acknowledges financial support from Award P200A120125 of the U.S. Department of Education Graduate Assistance in Areas of National Need Program as well as the U.S. National Science Foundation Graduate Research Fellowship (DGE 1144083). The authors would also like to thank the NSF CHE-MSN grant 1508728 and the NSF CHE-CAT grant 1800585 for financial support

#### Appendix A. Supplementary data

Supplementary material related to this article can be found, in the online version, at doi:<https://doi.org/10.1016/j.apcatb.2019.05.036>.

#### References

- [1] M. Cao, D. Wu, R. Cao, Recent advances in the stabilization of platinum electrocatalysts for fuel-cell reactions, *Chem. Cat. Chem.* 6 (2014) 26–45.
- [2] S.S. Kocha, Electrochemical degradation: electrocatalyst and support durability, in: M.M. Mench, E.C. Kumbur, T.N. Veziroglu (Eds.), *Polymer Electrolyte Fuel Cell Degradation*, Elsevier, Waltham, MA, 2012.
- [3] A.V. Virkar, Y. Zhou, Mechanism of catalyst degradation in proton exchange membrane fuel cells, *J. Electrochem. Soc.* 154 (2007) B540–B547.
- [4] H. Takenaka, K. Nakagawa, H. Matsune, E. Tanabe, M. Kishida, Improvement in the durability of Pt electrocatalysts by coverage with silica layers, *J. Phys. Chem. C Lett.* 111 (2007) 15133–15136.
- [5] S. Takenaka, T. Miyazaki, H. Matsune, M. Kishida, Highly active and durable silica-coated Pt cathode catalysts for polymer electrolyte fuel cells: control of micropore structures in silica layers, *Catal. Sci. Technol.* 5 (2015) 1133–1142.
- [6] K. Cheng, M. Jiang, B. Ye, I.S. Amiin, X. Liu, Z. Kou, W. Li, S. Mu, Three-dimensionally costabilized metal catalysts toward an oxygen reduction reaction, *Langmuir* 32 (2016) 2236–2244.
- [7] C. Yang, M. Zhou, M. Zhang, L. Gao, Mitigating the degradation of carbon-supported Pt electrocatalysts by tungsten oxide nanoplates, *Electrochim. Acta* 188 (2016) 529–536.
- [8] A.W. Weimer, Particle atomic layer deposition, *J. Nano. Res.* 21 (2019) 9.
- [9] J. Lu, J.W. Elam, P.C. Stair, Atomic layer deposition—sequential self-limiting surface reactions for advanced catalyst “bottom-up” synthesis, *Surf. Sci. Rep.* 71 (2016) 410–472.
- [10] H. Feng, J. Lu, P.C. Stair, J.W. Elam, Alumina over-coating on Pd nanoparticle catalysts by atomic layer deposition: enhanced stability and reactivity, *Catal. Letters* 141 (2011) 512–517.
- [11] X. Liang, J. Li, M. Yu, C.N. McMurray, J.L. Falconer, A.W. Weimer, Stabilization of supported metal nanoparticles using an ultrathin porous shell, *ACS Catal.* 1 (2011) 1162–1165.
- [12] T.D. Gould, A. Izar, A.W. Weimer, J.L. Falconer, J.W. Medlin, Stabilizing Ni catalysts by molecular layer deposition for harsh, dry reforming conditions, *ACS Catal.* 4 (2014) 2714–2717.
- [13] J. Lu, B. Fu, M.C. Kung, G. Xiao, J.W. Elam, H.H. Kung, P.C. Stair, Coking- and sintering-resistant palladium catalysts achieved through atomic layer deposition, *Science* 335 (2012) 1205–1208.
- [14] N. Cheng, Y. Shao, J. Liu, X. Sun, Electrocatalysts by atomic layer deposition for fuel cell applications, *Nano Energy* 29 (2016) 220–242.
- [15] N. Cheng, M.N. Banis, J. Liu, A. Riese, X. Li, R. Li, S. Ye, S. Knights, X. Sun, Extremely stable platinum nanoparticles encapsulated in a zirconia nanocage by area-selective atomic layer deposition for the oxygen reduction reaction, *Adv Mater* 27 (2015) 277–281.
- [16] C. Marichy, G. Ercolano, G. Caputo, M.G. Willinger, D. Jones, J. Rozière, N. Pinna, S. Cavaliere, ALD SnO<sub>2</sub> protective decoration enhances the durability of a Pt based electrocatalyst, *J. Mater. Chem. A* 4 (2016) 969–975.
- [17] W.W. McNeary, A.E. Linico, C. Ngo, S. van Rooij, S. Haussener, M.E. Maguire, S. Pylypenko, A.W. Weimer, Atomic layer deposition of TiO<sub>2</sub> for stabilization of Pt nanoparticle oxygen reduction reaction catalysts, *J. Appl. Electrochem.* 48 (2018) 973–984.
- [18] S. Chung, M. Choun, B. Jeong, J.K. Lee, J. Lee, Atomic layer deposition of ultrathin layered TiO<sub>2</sub> on Pt/C cathode catalyst for extended durability in polymer electrolyte fuel cells, *J. Energy Chem.* 25 (2016) 258–264.
- [19] Z. Song, M.N. Banis, L. Zhang, B. Wang, L. Yang, D. Banham, Y. Zhao, J. Liang, M. Zheng, R. Li, S. Ye, X. Sun, Origin of achieving the enhanced activity and stability of Pt electrocatalysts with strong metal-support interactions via atomic layer deposition, *Nano Energy* 53 (2018) 716–725.
- [20] J. Kim, S. Yang, H. Lee, Platinum–titanium intermetallic nanoparticle catalysts for oxygen reduction reaction with enhanced activity and durability, *Electrochem. Commun.* 66 (2016) 66–70.
- [21] D. Ham, J. Lee, Transition metal carbides and nitrides as electrode materials for low temperature fuel cells, *Energies* 2 (2009) 873–899.
- [22] E. Antolini, E.R. Gonzalez, Tungsten-based materials for fuel cell applications, *Appl. Catal. B* 96 (2010) 245–266.
- [23] A.M. Lubers, W.W. McNeary, D.J. Ludlow, A.W. Drake, M. Faust, M.E. Maguire,

- M.U. Kudas, M. Seipenbusch, A.W. Weimer, Proton exchange membrane fuel cell flooding caused by residual functional groups after platinum atomic layer deposition, *Electrochim. Acta* 237 (2017) 192–198.
- [24] J.S. Becker, R.G. Gordon, Diffusion barrier properties of tungsten nitride films grown by atomic layer deposition from bis(tert-butylimido)bis(dimethylamido) tungsten and ammonia, *Appl. Phys. Lett.* 82 (2003) 2239–2241.
- [25] J.S. Becker, S. Wang, R.G. Gordon, Highly conformal thin films of tungsten nitride prepared by atomic layer deposition from a novel precursor, *Chem. Mater.* 15 (2003) 2969–2976.
- [26] K. Shinozaki, J.W. Zack, R.M. Richards, B.S. Pivovar, S.S. Kocha, Oxygen reduction reaction measurements on platinum electrocatalysts utilizing rotating disk electrode technique, *J. Electrochem. Soc.* 162 (2015) F1144–F1158.
- [27] Y. Dai, L. Ou, W. Liang, F. Yang, Y. Liu, S. Chen, Efficient and superiorly durable Pt-Lean electrocatalysts of Pt–W alloys for the oxygen reduction reaction, *J. Phys. Chem. C* 115 (2011) 2162–2168.
- [28] Y. Wang, Y. Yang, L. Zou, Q. Huang, Q. Li, Q. Xu, H. Yang, Carbon-supported W@Pt nanoparticles with a Pt-Enriched surface as a robust electrocatalyst for oxygen reduction reactions, *ChemistrySelect* 3 (2018) 1056–1061.
- [29] R.T. Downs, M. Hall-Wallace, The american mineralogist crystal structure database, *Am. Mineral.* 88 (2003) 247–250.
- [30] P.L. Moharana, S. Anwar, A. Islam, S. Anwar, Structural and mechanical study of thermally annealed tungsten nitride thin films, *Perspect. Sci.* 8 (2016) 636–638.
- [31] S. Mukerjee, Particle size and structural effects in platinum electrocatalysis, *J. Appl. Electrochem.* 20 (1990) 537–548.
- [32] G.S. Karlberg, T.F. Jaramillo, E. Skulason, J. Rossmeisl, T. Bligaard, J.K. Nørskov, Cyclic voltammograms for H on Pt(111) and Pt(100) from first principles, *Phys. Rev. Lett.* 99 (2007) 126101.
- [33] J.L. Shim C-R, H.-K. Lee, J.-S. Lee, E.J. Cairns, Electrochemical characteristics of Pt-WO<sub>3</sub>/C and Pt-TiO<sub>2</sub>/C electrocatalysts in a polymer electrolyte Fuel Cell, *J. Power Sources* 102 (2001) 172–177.
- [34] N.R. Elezovic, B.M. Babic, P. Ercius, V.R. Radmilovic, L.M. Vracar, N.V. Krstajic, Synthesis and characterization Pt nanocatalysts on tungsten based supports for oxygen reduction reaction, *Appl. Catal. B* 125 (2012) 390–397.
- [35] O. Alexeev, M. Shelef, B.C. Gates, MgO-supported platinum-tungsten catalysts prepared from organometallic precursors: platinum clusters isolated on dispersed tungsten, *J. Catal.* 164 (1996) 1–15.
- [36] R. Liu, D. Wu, X. Feng, K. Mullen, Nitrogen-doped ordered mesoporous graphitic arrays with high electrocatalytic activity for oxygen reduction, *Angew. Chemie Int. Ed.* 49 (2010) 2565–2569.